Concurrent Testing of Digital Microfluidics-Based Biochips

FEI SU, SULE OZEV, and KRISHNENDU CHAKRABARTY
Duke University

We present a concurrent testing methodology for detecting catastrophic faults in digital microfluidics-based biochips and investigate the related problems of test planning and resource optimization. We first show that an integer linear programming model can be used to minimize testing time for a given hardware overhead, for example, droplet dispensing sources and capacitive sensing circuitry. Due to the NP-complete nature of the problem, we also develop efficient heuristic procedures to solve this optimization problem. We apply the proposed concurrent testing methodology to a droplet-based microfluidic array that was fabricated and used to perform multiplexed glucose and lactate assays. Experimental results show that the proposed test approach interleaves test application with the biomedical assays and prevents resource conflicts. The proposed method is therefore directed at ensuring high reliability and availability of bio-MEMS and lab-on-a-chip systems, as they are increasingly deployed for safety-critical applications.

Categories and Subject Descriptors: B.7.2 [**Integrated Circuits**]: Design Aids—*Simulation*; B.8.1 [**Performance and Reliability**]: Reliability, Testing, and Fault-Tolerance; J.3 [**Life and Medical Sciences**]: *Biology and genetics, health*

General Terms: Algorithms, Performance, Design, Reliability

Additional Key Words and Phrases: Concurrent testing, catastrophic faults, microfluidics, biochips

1. INTRODUCTION

Microfluidics-based biochips for biochemical analysis have become popular in recent years [Srinivasan et al. 2004; Thorsen et al. 2002; Zhang et al. 2002]. These composite microsystems, also known as bio-MEMS or lab-on-a-chip (LoC), offer several advantages over macroscopic systems, such as design flexibility, smaller size, lower cost, and higher sensitivity. They enable the control of small amounts (e.g., micro- and nano-liters) of fluids, thus reducing

The work of F. Su and K. Chakrabarty was supported in part by the National Science Foundation (NSF) under grant number IIS-0312352.
A preliminary and abridged version of this article was published in *Proceedings of the IEEE International Test Conference*, IEEE Computer Science Press, Los Alamitos, CA, 2004, pp. 883–892.
Authors' address: Department of Electrical and Computer Engineering, Duke University, Durham, NC, 27708; email: {fs,sule,krish}@ee.duke.edu.

sample size and reagent volume as well as power consumption. Advances in microfluidic techniques offer exciting possibilities in the realm of massively parallel DNA analysis, automated drug synthesis, and real-time biomolecular detection and recognition. Clinical diagnosis is one of the most promising applications for these techniques [Davies 1995; Schulte et al. 2002]. Miniaturization in microfluidics can offer immediate point-of-care diagnosis of diseases. Moreover, techniques to counter bioterrorism can tremendously benefit from microfluidics [Hull et al. 2003; Paul 2002; Venkatesh and Memish 2003]. Such microfluidics-based systems, capable of continuous sampling and real-time testing of air/water samples for biochemical toxins and other pathogens, can serve as an always-on "bio-smoke alarm" to offer an early warning capability to combatants or citizens.

Currently, most microfluidic biochips, consisting of micro-pumps, microvalves, and micro-channels, are based on the principle of continuous fluid flow [Henning 1998; Verpoorte and de Rooij 2003]. A promising alternative paradigm involves the manipulation of liquids as discrete microdroplets [Cho et al. 2002; Pollack et al. 2000]. Following the analogy of microelectronics, this novel approach is referred to as "digital microfluidics". The digital microfluidics-based biochips enable easy reconfigurability since each droplet can be controlled independently and each cell in the array has the same structure. The feasibility of performing real-time biomedical assays, for example, the colorimetric enzyme-kinetic glucose assay or the polymerase chain reaction (PCR), on these novel microsystems has recently been demonstrated experimentally [Pollack et al. 2003; Srinivasan et al. 2003a, 2003b].

As digital microfluidics-based biochips are widely deployed in safety-critical biomedical applications, the reliability of these systems has emerged as a critical performance parameter. These systems need to be tested adequately not only after fabrication, but also continuously during in-field operation. For instance, for detectors monitoring for dangerous pathogens in critical locations such as airports, field testing is critical to ensure low false-positive and false-negative detection rates. In such cases, concurrent testing, which allows testing and normal biomedical assays to run simultaneously on a microfluidic system, can play an important role. It consequently facilitates built-in self-test (BIST) of microfluidics-based biochips and makes them less dependent on costly manual maintenance on a regular basis.

Next-generation system-on-chip designs are expected to be composite microsystems incorporated with microelectromechanical and microfluidic components. Therefore, there is a need for efficient testing methodologies for these mixed-technology microsystems. The ITRS 2003 document recognizes the need for new test methods for disruptive device technologies that underly composite microsystems, and highlights it as one of the five difficult test challenges beyond 2009 [ITRS].

A cost-effective test methodology for digital microfluidic systems was first described in Su et al. [2005]. Likely physical defects in such systems were analyzed and faults were classified as being either catastrophic or parametric. Faults are detected in Su et al. [2005] by electrically controlling and tracking the motion of test droplets. This cost-effective test methodology necessitates

concurrent testing for digital microfluidics-based biochips. Test planning and resource optimization are motivated by the need for concurrent testing. An optimal test planning method based on graph theory was investigated in Su et al. [2004] in which a digital microfluidic array is simply divided into two parts: the cells used in bioassays (i.e., primary cells) and the unused cells (i.e., spare cells). The proposed testing procedure is only applied to the spare cells, and the cells used for bioassays are considered to be unavailable for testing. However, in real-life bioassays, most cells used for assay operations are not occupied by sample or reagent droplets at all times. This implies that they may still be available for testing in some particular time period. Therefore, we can further perform an efficient concurrent testing to allow test droplets to detect the cells used in bioassay following a carefully designed test plan, when the schedule of bioassay is known *a priori*.

In this article, we present such a concurrent testing methodology for detecting catastrophic faults in digital microfluidics-based biochips. An integer linear programming (ILP) model is first formulated to derive an optimal droplet flow path for concurrent testing. Due to the $\mathcal{NP}$-completeness of the problem, the ILP model is not applicable to large microfluidic arrays. We therefore develop heuristics to solve this problem in a computationally efficient manner. This concurrent testing methodology is evaluated by using a real-life digital microfluidics-based biochip performing multiplexed biomedical assays. We present test plans that interleave test application with the set of biochemical assays and prevent the resource conflicts. Even though the methodology described herein is applied to only catastrophic faults, it can easily be extended for the detection of parametric faults as described in Su et al. [2005].

The organization of the remainder of the article is as follows: In Section 2, we present an overview of digital microfluidics-based biochips and a multiplexed biomedical assay that can be performed on such systems. Next, a concurrent testing methodology to facilitate in-field monitoring is discussed in Section 3. Related prior work is discussed in Section 4. Section 5 presents an integer linear programming (ILP) model based on the notion of scheduling using time-slots. We minimize the test application time for a given hardware overhead by optimizing the test plan using the ILP model. To deal with large microfluidic arrays, several heuristic algorithms are presented in Section 6. Section 7 evaluates the proposed concurrent testing methodology by applying it to a digital microfluidic biochip used for multiplexed biomedical assays. Finally, conclusions are drawn in Section 8.

2. DIGITAL MICROFLUIDICS-BASED BIOCHIPS AND MULTIPLEXED BIOMEDICAL ASSAYS

The microfluidic system discussed in this article is based on the manipulation of nanoliter droplets using the principle of electrowetting. Electrowetting is a phenomenon whereby an electric field can modify the wetting behavior of a droplet in contact with an insulated electrode. If an electric field is applied non-uniformly, then a surface energy gradient is created which can be used to manipulate a droplet sandwiched between two plates [Pollack et al. 2000]. By

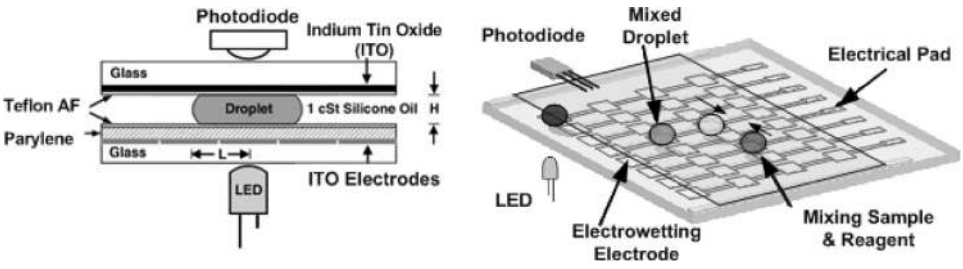

Fig. 1. Digital microfluidics-based biochips used in colorimetric enzyme-kinetic assay.

varying the electrical potential along a linear array of electrodes, electrowetting can be used to move nanoliter volume liquid droplets along this line of electrodes [Pollack et al. 2000]. Droplets can also be transported, in user-defined patterns and under clocked-voltage control, over a two-dimensional array of electrodes without the need for micropumps and microvalves.

The advantages of reduced reagent consumption, simplicity of sensing, and rapid analysis facilitate the widespread deployment of digital microfluidic biochips in a clinical point-of-care setting. The *in-vitro* measurement of glucose and other metabolites, such as lactate, glutamate and pyruvate, is of great importance in clinical diagnosis of metabolic disorders. Recently, a colorimetric enzyme-kinetic glucose assay performed on the droplet-based microfluidic system has been successfully demonstrated [Srinivasan et al. 2003a, 2003b; Videos]. This system uses a basic microfluidic platform, which moves and mixes droplets containing biomedical samples and reagents, and an integrated optical detection system consisting of a LED and a photodiode; see Figure 1 [Srinivasan et al. 2003a, 2003b].

The basic cell of a digital microfluidic array consists of two glass plates. The bottom plate contains a patterned array of individually controllable electrodes, and the top plate is coated with a continuous ground electrode; all electrodes are formed by indium tin oxide (ITO). The droplets travel inside the filler medium, that is, silicone oil, sandwiched between the plates. An 800-nm-thick dielectric insulator, that is, parylene C, coated with a 60-nm-thick hydrophobic film of Teflon AF, is added to the plates to decrease the wettability of the surface and to add capacitance between the droplet and the control electrode. The length of the control electrode L is 1.5 mm and the height between two plates H is 0.475 mm [Srinivasan et al. 2003a]. The detailed fabrication process is described in [Pollack et al. 2002]. The basic principle of droplet transportation is to electrically control the interfacial tension at the droplet/insulator interface. A control voltage is applied to an electrode adjacent to the droplet and at the same time the electrode just under the droplet is deactivated. This causes an accumulation of charge in the droplet/insulator interface, resulting in a tension gradient across the gap between the adjacent electrodes, which consequently causes the droplet motion. The velocity of the droplet can be controlled by adjusting the control voltage (0∼90V), and droplets can be moved at speeds of up to 20 cm/s. Based on this principle, droplets can be moved freely to any location of a two-dimensional microfluidic array. Note

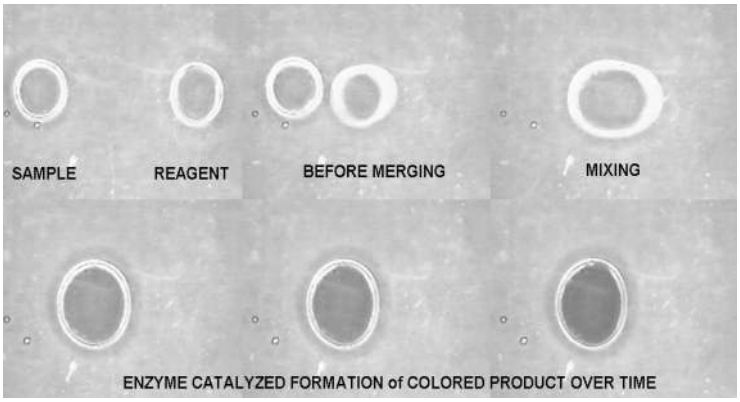

Fig. 2. Photos in different steps of a real-life droplet-based glucose assay.

that in the glucose assay experiment, the actuation voltage was set at 50 V [Srinivasan et al. 2003a].

The glucose assay performed on the digital microfluidic biochip is based on Trinder's reaction, a colorimetric enzyme-based method [Trinder 1969]. The enzymatic reactions involved in the assay are:

$$\text{Glucose} + H_2O + O_2 \xrightarrow{\text{Glucose Oxidase}} \text{Gluconic Acid} + H_2O_2$$

$$2H_2O_2 + 4 - \text{AAP} + \text{TOPS} \xrightarrow{\text{Peroxidase}} \text{Quinoneimine} + 4H_2O$$

In the presence of Glucose oxidase, glucose can be enzymatically oxidized to gluconic acid and hydrogen peroxide. Then, in the presence of peroxidase, the hydrogen peroxide reacts with 4-amino antipyrine (4-AAP) and N-ethyl-N-sulfopropyl-m-toluidine (TOPS) to form violet-colored quinoneimine, which has an absorbance peak at 545 nm. Based on this colorimetric reaction, the complete glucose assay can be performed following three steps, namely, transportation, mixing and optical detection; see Figure 2 [Videos]. Sample droplets containing glucose and reagent droplets containing glucose oxidase, peroxidase, 4-AAP and TOPS, are dispensed into the microfluidic system from droplet sources. They are then transported towards a mixer where droplets of the sample and the reagent are mixed together and the enzymatic reaction happens during the mixing. A droplet of the product after mixing is moved to the location of optical detection. The optical detection is performed using a green LED and a photodiode. The glucose concentration can be detected from the absorbance, which is related to the concentration of colored quinoneimine, using a kinetic method. In the kinetic method, the concentration of the glucose is calculated from the rate of the reaction, which is equivalent to the rate of the change of absorbance. The details of the kinetic method for optical detection can be found in [Srinivasan et al. 2003a]. Experiments have shown that the results from the digital microfluidics-based biochips match well with the reference values obtained from the conventional measurement, with a relative error of less than 10% [Srinivasan et al. 2003a, 2003b].

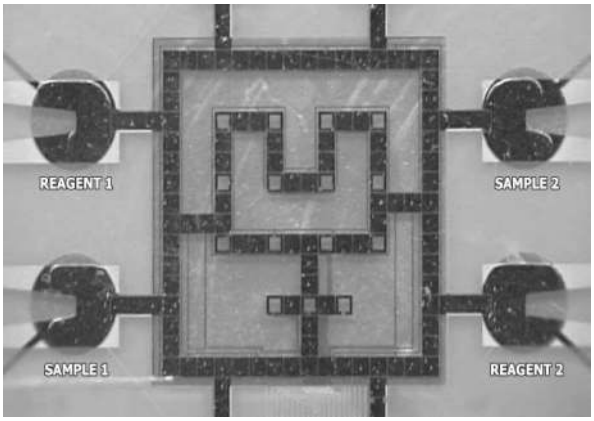

Fig. 3. Fabricated microfluidic array used in multiplexed bioassays.

In addition to glucose assays, the detections of other metabolites such as lactate, glutamate and pyruvate in a digital microfluidics-based biochip have also been demonstrated recently [Srinivasan et al. 2003a, 2003b]. Using similar enzymatic reactions and modified reagents, these assays as well as the glucose assay can be integrated to form a multiplexed biomedical assay performed concurrently on a droplet-based microfluidic system. Figure 3 shows an image of such a fabricated microfluidic system used for multiplexed biomedical assays. Sample1 contains glucose and Reagent1 contains glucose oxidase and other chemicals. Similarly, Sample2 contains lactate and Reagent2 consists of lactate oxidase and other chemicals. To demonstrate multiplexed assays, only cells and electrodes used for the biomedical assay have been fabricated. In addition, on-chip reservoirs are integrated to automatically dispense sample and reagent droplets into the microfluidic array [Srinivasan et al. 2003a].

3. RELATED PRIOR WORK

Over the past decade, the focus in testing research has broadened from logic and memory test to include the testing of analog and mixed-signal circuits. MEMS is a relatively young field compared to IC design, and MEMS testing is still in its infancy. Recently, fault modeling and fault simulation in surface micromachined MEMS has received attention [Dhayni et al. 2004; Dumas et al. 2004; Mir et al. 2000]. In Deb and Blanton [2000, 2004] and Kerkhoff [1996], a comprehensive testing methodology for a class of MEMS known as surface micromachined sensors is presented.

However, test techniques for MEMS cannot be directly applied to microfluidic systems, since they differ in the underlying energy domains and in their working principles. The techniques and tools currently in use for the testing of classical MEMS (e.g., comb-drive microresonator) mainly aim at mechanical defects such as stiction; they do not handle fluids. Thus, new testing techniques are required for microfluidics-based biochips. Very limited work has been reported in this area. Recently, fault modeling and fault simulation for continuous-flow microfluidic biochips have been proposed in Kerkhoff [1999] and Kerkhoff and

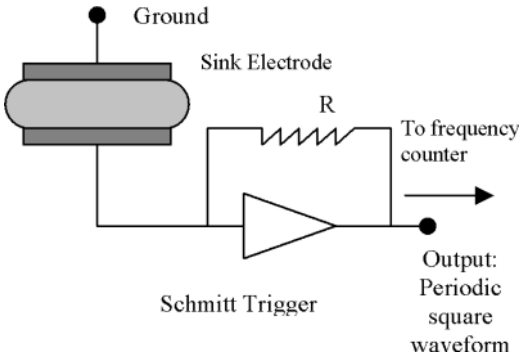

Fig. 4. Simple capacitive sensing circuit.

Acar [2003]. Also, a DFT technique for Flow-FET-based microfluidic systems has been discussed in Kerkhoff and Hendriks [2001]. Similar to MOSFET, a Flow-FET has source and drain electrodes over which a relatively large voltage ($\sim$100V) is applied. Due to the principle of electro-osmotic flow, the electric field moves the charge accumulated between the fluid and the surface of channel, dragging the bulk liquid through the channel.

4. CONCURRENT TESTING METHODOLOGY

Based on the detection mechanism proposed in Su et al. [2005], we dispense the test droplet containing a conductive fluid (e.g., KCL solution) into the microfluidic chip-under-test (CUT) from the droplet source. These droplets are guided through the cells of the microfluidic array following the test plan towards the droplet sink, which is connected to an integrated capacitive detection circuit. An example of such a capacitive detection circuit is shown in Figure 4, which consists of a simple RC oscillator circuit formed by the sink electrodes and the fluid between them as an insulator. The capacitance of this structure depends on the presence of the droplet since the filler medium and the droplet have distinct permittivities. By sensing the capacitance of this structure through a simple frequency counter, one can determine whether a droplet has reached the sink. This mechanism can be electronically implemented and easily integrated on-chip. Most catastrophic faults result in a complete cessation of droplet transportation. Thus, for the faulty system, the test droplet is stuck during its motion. On the other hand, for the fault-free system, all test droplets can be observed at the droplet sink by the capacitive detection circuit. Therefore, we can easily determine the fault-free or faulty status of a digital microfluidics-based biochip by simply observing the arrival of test droplets at some selected ports of the system.

This cost-effective fault testing procedure can be performed simultaneously with a normal biochemical assay on a microfluidic system. The goals and constraints of the concurrent testing problem are as follows:

(1) *Concurrency*. The test plan should ensure simultaneous execution of the test procedures and biochemical assays, and there are no conflicts between them.

(2) *Optimization*. There exists an inherent tradeoff between hardware overhead and test application time. Here the hardware overhead is measured by the number of test droplet sources and droplet sinks for test application. For a given hardware overhead, test application time should be minimized, which allows a biochip to report its faulty status as early as possible during concurrent testing.

(3) *Full coverage*. Cells in the microfluidic array that are not occupied by sample or reagent samples for bioassays are available for testing. The test plan should cover all cells in the microfluidic array.

The proposed concurrent testing methodology can be used for field-testing of digital microfluidics-based biochips; as a result, it increases the system reliability during everyday operation. With negligible hardware overhead, this method also offers an opportunity to implement BIST for microfluidic systems and therefore eliminate the need for costly, bulky, and expensive external test equipment. Furthermore, after detection, droplet flow paths for bioassays can be reconfigured dynamically such that faulty cells are bypassed without interrupting the normal operation [Su and Chakrabarty 2005]. Thus, this approach increases fault-tolerance and system lifetime when such systems are deployed for safety-critical applications.

5. OPTIMAL SCHEDULING FOR CONCURRENT TESTING

In this section, we formulate the problem of test planning for concurrent testing. The key idea underlying this optimization method is based on the notion of time slots. In order to determine the droplet flow paths, we divide the total test time into equal-length time slots. The length of a time slot equals the time during which a test droplet moves from a cell to an adjacent cell. The goal of the optimal scheduling problem (OSP) developed in this section is to determine all the time slots at which the microfluidic cells are visited by the test droplets, such that the total time cost that is, the time slot at which droplets reach the sinks after visiting all cells in the array, is minimized.

Although the above scheduling problem can be easily shown to be $\mathcal{NP}$-complete using Graham et al. [1979], we show that this problem can be solved exactly for a microfluidic array of modest size using integer linear programming (ILP) model. Here, we first consider the case of one single test droplet. An ILP model can be described as follows:

Minimize: Ax (objective function)
Subject to: $Bx \leq C$ (constraint inequalities),

where x is a vector of variables, A is an objective function vector, B is a constraint matrix and C is a column vector of constraints. A popular public domain ILP solver called *lpsolve* is used in this article [Berkelaar].

Here we use the example of Figure 5 as an illustration to formulate this ILP model. White squares denote cells that are not used by the bioassay and are therefore available for testing. The black cells are occupied by sample or reagent droplets for an assay operation such as droplet mixing or storage, therefore they are temporarily unavailable for testing. Every cell is represented by

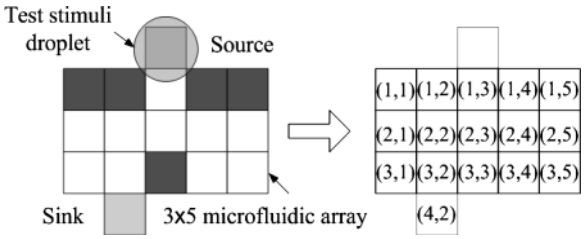

Fig. 5. Coordinate representation of an array of cells.

two-dimensional coordinates (i, j), where i is the row number and j is the column number of the cell; see Figure 5.

Let X_{ijk} be a binary variable defined as follows:

$$X_{ijk} = \begin{cases} 1 \text{ if cell } (i, j) \text{ is visited by a droplet at time slot } k \\ 0 \text{ otherwise} \end{cases}$$

where $1 \leq k \leq T$. The parameter T is the maximum possible index for a time slot and its value can be set to an easily-determined loose upper bound.

In the example of Figure 5, cell (4, 2) is a sink. Since the sink should be visited exactly once during test application, $\sum_{k=1}^{T} X_{42k} = 1$. Thus, the time slot at which a test droplet reaches this sink, that is, all testing operations have been finished, is $C = \sum_{k=1}^{T} k \times X_{42k}$.

Hence, the objective function of the ILP model for OSP is

$$\text{minimize: } C = \sum_{k=1}^{T} k \times X_{42k}.$$

The following constraint inequalities need to be incorporated into this model.

(1) *Testing requirement.*
   (a) $\sum_{k=1}^{T} X_{ijk} \geq 1$,for $(i, j) \in \{AT$: set of cells available for testing$\}$, that is, any cell (i, j) in the array available for testing should be visited by the test droplet at least once
   (b) $\sum_{k=1}^{T} X_{ijk} = 0$,for $(i, j) \in \{NAT$: set of cells not available for testing$\}$,that is, any cell (i, j) in array that is running biomedical assays cannot be visited by the test droplet.
   (c) $\sum_{k=1}^{T} X_{42k} = 1$, that is, the sink (the cell (4,2) in here) should be visited by the test droplet exactly once.

(2) *Resource constraint*. Consider the case of one single test droplet. Before the test droplet reaches the sink, only one cell in the array can be visited by this droplet in any time-slot. After that, no cells in the array (including the sink) can be visited by a test droplet again before a new test application procedure starts. This constraint for an $m \times n$ array (a 3×5 array is shown here) can be modeled as follows:

$$\sum_{i=1}^{m} \sum_{j=1}^{n} X_{ijk} = 1 - \sum_{t=1}^{k-1} X_{42t} = \begin{cases} 1 \text{ otherwise} \\ 0 \text{ if } X_{421} - 1, t \leq k - 1 \end{cases}$$

where $2 \leq k \leq T$.

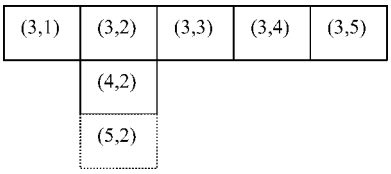

Fig. 6. Virtual cell added to the array of Figure 5.

To simplify the model, an additional virtual cell is added adjacent to the sink. The test droplet is viewed as being finally stored in this virtual cell after test application. In the running example of Figure 5, the virtual cell (5, 2) is added; see Figure 6.

The above constraint can now be expressed as:

(a) $\sum_{i=1}^{m}\sum_{j=1}^{n} X_{ijk} = 1$,where $1 \leq k \leq T$, and (i, j) is any cell in the microfluidic array, including virtual cell (5,2).

(b) $X_{52k} = \sum_{t=1}^{k-1} X_{42t}$,where $2 \leq k \leq T$.

(3) *Starting point.* This is determined by the location of the droplet source. In our example, $X_{131} = 1$, that is, the cell (1, 3) is visited by the test droplet at time slot 1.

(4) *Movement rules*. When the test droplet moves in the microfluidic array, it should obey the movement rules described as follows. It only can move to its neighbors, that is, if the droplet visits cell (i, j) at time slot k, then for time slot $k + 1$, the droplet can only move to column $j + 1$, j, or $j - 1$ when it remains in the same row i. Similarly, if it stays in the same column j, the possible rows in time slot $k + 1$ are $i - 1$, i, or $i + 1$.

This rule can be modeled as follows:

Let $P_k = \sum_{i=1}^{m}\sum_{j=1}^{n} i \times X_{ijk}$ be the number of the row visited at time-slot k. Likewise, let $q_k = \sum_{i=1}^{m}\sum_{j=1}^{n} j \times X_{ijk}$ be the number of the column visited at time-slot k. Let $\Delta P_k = |P_{k+1} - P_k|$ and $\Delta q_k = |q_{k+1} - q_k|$. We must ensure that $\Delta P_k + \Delta q_k \leq 1$.

We have now developed the ILP model for OSP using Figure 5 as a running example. The general ILP model for an $m \times n$ array is shown in Figure 7, where cell (a, b) refers to the test droplet sink and cell (c, d) is adjacent to the test droplet source. The complexity of this model is O(mnT) in the number of variables and O($mn + T$) in the number of constraints for an $m \times n$ array. The result obtained using *lpsolve* for Figure 5 is shown in Table I. It took 5 minutes of CPU time with a 1.0GHz Pentium-III PC with 256 MB of RAM. The optimal test schedule for this 3×5 array generated by *lpsolve* is shown in Figure 8, where the number in the cell represents the time slot. We notice that some cell, for example, cells (2, 3) and (2, 4) in Figure 5, need to be visited more than once by the test droplet.

The ILP model for OSP can easily be extended to find an optimal test schedule for more than one source and more than one sink as follows:

minimize: $C = \sum_{k=1}^{T} k \times X_{abk}$

Subject to:

1) $\sum_{k=1}^{T} X_{ijk} \geq 1$, *for any cell (i, j) available for testing.*

2) $\sum_{k=1}^{T} X_{ijk} = 0$, *for any cell (i, j) that is running biomedical assays and not available for testing.*

3) $\sum_{k=1}^{T} X_{abk} = 1$, *for the sink, that is the cell (a, b)*

4) $\sum_{i=1}^{m} \sum_{j=1}^{n} X_{ijk} = 1$, *where* $1 \leq k \leq T$, *and (i, j) is any cell in the microfluidic array, including virtual cell* (a^*, b).

5) $X_{a^*bk} = \sum_{t=1}^{k-1} X_{abt}$, *where* $2 \leq k \leq T$.

6) $X_{cd1} = 1$

7) $P_k = \sum_{i=1}^{m} \sum_{j=1}^{n} i \times X_{ijk}$ $q_k = \sum_{i=1}^{m} \sum_{j=1}^{n} j \times X_{ijk}$

8) $\Delta P_k = |P_{k+1} - P_k|$ $\Delta q_k = |q_{k+1} - q_k|$

9) $\Delta P_k + \Delta q_k \leq 1$

Fig. 7. Integer linear programming model for an $m \times n$ array.

Table I. Optimization Result for OSP for the Example of Figure 5 (Only variables assigned the value 1 are listed)

Variables	Value	Variables	Value
Objective function	13	X_{247}	1
C	13	X_{238}	1
X_{131}	1	X_{229}	1
X_{232}	1	X_{2110}	1
X_{243}	1	X_{3111}	1
X_{254}	1	X_{3212}	1
X_{355}	1	X_{4213}	1
X_{346}	1	X_{5214}	1

We modify the binary variable X_{ijk} to X_{ijkl} as follows:

$$X_{ijkl} = \begin{cases} 1 & \text{if cell } (i, j) \text{ is visited by test droplet } l \text{ at time slot } k \\ 0 & \text{otherwise,} \end{cases}$$

where $1 \leq k \leq T$, $1 \leq l \leq N$, and N is the number of source-sink pairs. (N= 2 in example of two droplet sources and two droplet sinks; see Figure 9). This ILP model is similar to the above model for OSP, with the following differences.

(1) The objective function is modified to minimize the maximum value of the time when each test droplet reaches its sink. For the example of Figure 9,

$$C = \max \left\{ \sum_{k=1}^{T} k \times X_{42k1}, \sum_{k=1}^{T} k \times X_{42k2} \right\}$$

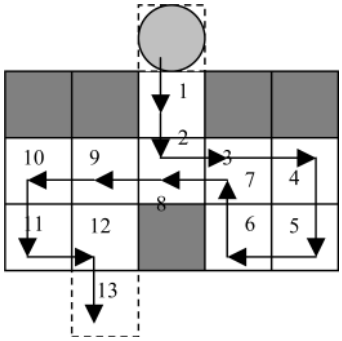

Fig. 8. Optimal test schedule for the example of Figure 5.

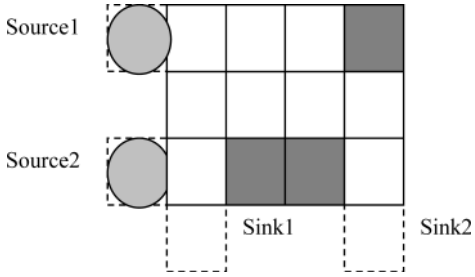

Fig. 9. Example of an array with two droplet sources and two droplet sinks.

(2) An additional constraint is incorporated as follows. Any cell (i, j) in the array cannot be visited by more than one test droplet at the same time slot, that is, $\sum_{l=1}^{N} X_{ijkl} \leq 1$ where $1 \leq k \leq T$. In the example of Figure 9, this is expressed as: $X_{ijk1} + X_{ijk2} \leq 1$.

(3) When multiple test droplets are applied, each droplet can never be in a cell directly adjacent or diagonally adjacent to another droplet. Otherwise, undesirable liquid mixing may occur in the array. This restriction prevents two droplets from mixing together. It can be expressed as:

$$\text{(a) } P_{kl} = \sum_{i=1}^{m}\sum_{j=1}^{n} i \times X_{ijkl}; q_{kl} = \sum_{i=1}^{m}\sum_{j=1}^{n} j \times X_{ijkl}\ l = 1, 2; \text{(b) } \Delta P_{k12} = |P_{k2} - P_{k1}|;$$
$$\Delta q_{k12} = |q_{k2} - q_{k1}|;\ \text{(c) } \Delta P_{k12} \geq 2, \text{or } \Delta q_{k12} \geq 2.$$

The optimized result obtained using *lpsolve* for the example of Figure 9 is listed in Table II. The ILP method took 15 minutes of CPU time. The test plan and the droplet paths based on the output of *lpsolve* are shown in Figure 10.

We can further modify the ILP model for OSP to derive a test plan that can support efficient concurrent testing during the execution of a biomedical assay, if its assay operation schedule is known *a priori* [Su and Chakrabarty 2004]. Note that the cells that are used in a bioassay operation, and viewed as unavailable cells in a particular time period, may still be available for testing in another time period. Let U_k be the set of cells, where each such cell is denoted by the pair (i, j), used by the assay in time slot k. Instead of setting $\sum_{k=1}^{T} X_{ijkl} = 0$

Table II. Optimization Result for OSP for the Example of Figure 9 (Only variables assigned the value 1 are listed)

Variable	Value	Variable	Value
Objective function	8	X_{4181}	1
C	8	X_{1112}	1
X_{3111}	1	X_{1222}	1
X_{3121}	1	X_{1332}	1
X_{2131}	1	X_{2342}	1
X_{2141}	1	X_{2452}	1
X_{2251}	1	X_{3462}	1
X_{2161}	1	X_{4472}	1
X_{3171}	1	X_{5482}	1

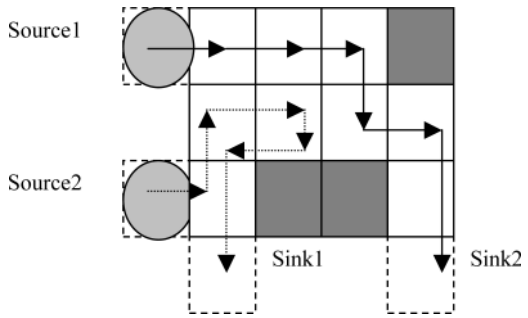

Fig. 10. Test droplet flow paths for the example of Figure 9.

for these cells for $1 \leq k \leq T$, we set $\sum_{(i,j)\in U_k} X_{ijkl} = 0$ for every time slot k. Thus, the ILP model can easily derive a concurrent test plan to test every cell, including primary cells and spare cells, in a digital microfluidic array.

6. HEURISTIC ALGORITHMS

We have shown in Section 5 that an ILP model can be formulated to solve the optimization problem of concurrent test planning exactly for a microfluidic array of modest size. Due to the computational complexity inherent in the optimal scheduling problem, however, there is a need for heuristic algorithms that can scale for large problem instances. We next propose two heuristic algorithms for the scheduling problem.

6.1 Scanning Path-Based Algorithm (SP)

In this heuristic approach, we first determine a simple scanning path of the test droplet on a digital microfluidic array, irrespective of the bioassay operation. This flow path, starting from the test droplet source and ending at the droplet sink, is designed to cover every cell in the array; one such example is shown in Figure 11. During concurrent testing, a test droplet is guided to visit the available microfluidic cell following the previously determined path. If the target cell is temporarily unavailable for test, that is, it is occupied by or adjacent to the bioassay droplet, the test droplet should wait in the current position until the target cell becomes available to visit. In the worse case, the test droplet has

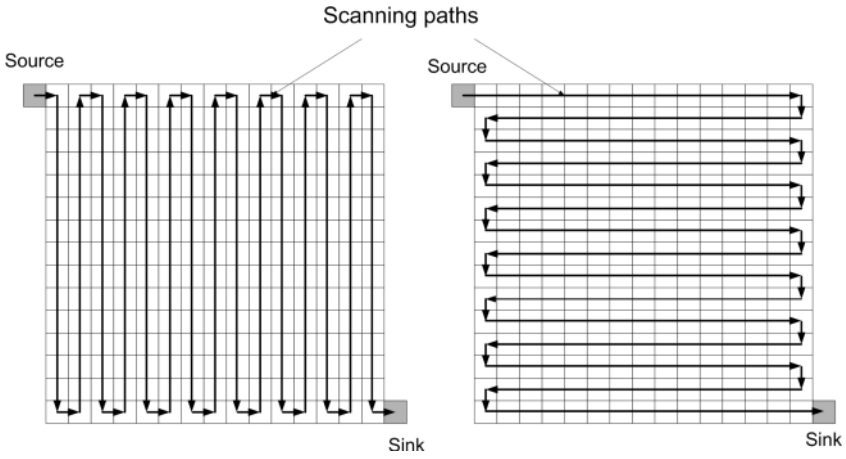

Fig. 11. Example of scanning paths used in the SP algorithm.

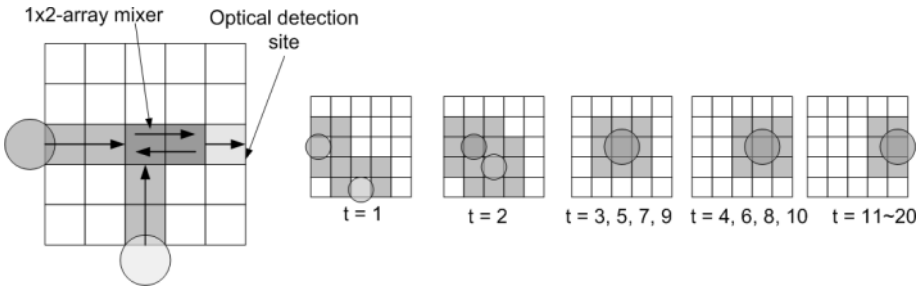

Fig. 12. Illustration example of heuristic approach.

to move back to the previous cell in order to avoid a conflict with the normal bioassay. Thus, the total testing time is equal to the sum of the tour time for the previously determined path and the additional time required for either waiting or turning back.

We next use the example of Figure 12 to illustrate how a concurrent test plan is obtained using the scanning path-based heuristic approach. In this example, one sample droplet (e.g., glucose fluid) and one reagent droplet (e.g., glucose oxidase and other chemicals) are first dispensed into a 5×5 array, and then mixed together in a simple 2-electrode linear array mixer. After mixing, the product droplet is relocated for optical detection. The bioassay schedule based on the notion of time-slots is also shown in Figure 12, whereby gray squares represent cells that are used by or are adjacent to the bioassay droplet in each time slot. A concurrent test plan can easily be obtained by using the SP algorithm; it took 1 minute of CPU time, as shown in Figure 13, where a test droplet is guided to scan this 5×5 array following a Hamiltonian path. Note that, in order to avoid conflict, the test droplet not only should wait at time slot 2 and 20, but it also has to move back at time slot 9. The total time for this test plan is 29 time slots.

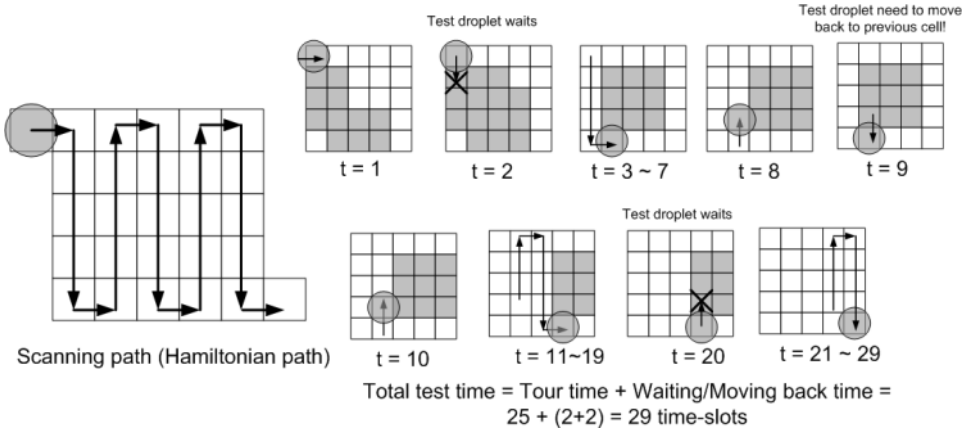

Fig. 13. The concurrent test plan obtained by the SP algorithm.

The main advantage of the SP algorithm is that it is easy to implement. A simple scanning path can be applied for a microfluidic array that is used in various bioassay operations; the concurrent testing plan can easily be obtained with low computation cost. Note that in some cases, however, the test droplet has to wait for a long time if the target cell is used by a time-consuming assay operation (e.g., optical detection), thereby leading to an excessively high testing time.

6.2 Modified Node-Counting Search Algorithm (MNCS)

To avoid the above cases in the SP approach, we can leverage probabilistic node-counting search algorithms for concurrent test planning [Balch and Arkin 1993]. The basic idea underlying this heuristic method is to carry out a number of simulation runs to heuristically find a feasible test plan. In each run, the test droplet starts from the cell directly adjacent to the test droplet source and ends in the droplet sink. It moves to the neighboring cell based on some rules as follows. This heuristic introduces an evaluation function U associated with each cell of a microfluidic array under test. When one cell is visited by the test droplet, the U-value of this cell is updated according to a predefined rule, that is, $U(\text{new}) = 1 + U(\text{old})$. Thus, this node counting method interprets the U-value as the number of times the location has been visited. In each time step, a set of neighboring cells available for test is first found. Then the test droplet greedily moves to an adjacent cell with the smallest U-value from this set. Ties due to same U-value neighbors are broken randomly if $U > 0$, that is, they have already been visited by the test droplet before. In the cases that $U = 0$, we further add a new evaluation function *Prior* to select the target from the set of untested cells. As in Su et al. [2004], we define the cells that are used by or adjacent to the bioassay droplets to be primary cells; otherwise, they are referred to as spare cells. If an untested cell is a primary cell and also it will be used by the normal bioassay after the current time-slot, a priority value of this cell is set as *Prior* = (Starting time of assay in this cell—current

MNCS: Modified node-counting search algorithm

```
1  /* Initialization (for an m×n microfluidic array) */
2  CellUsed(i, j) = 1 if this cell is used in bioassay or as an isolation wrapper, i.e., it is a primary cell;
   CellUsed(i, j) = 0 if this cell is a spare cell
3  Acell(i, j, t) = 1 if cell(i, j) is not available for testing at time slot t;
   Acell(i, j, t) = 0 if cell(i, j) is available for testing at time slot t;
4  Starting point of a test path is determined by the source location;
   Stopping point is determined by the sink location
5  Loop: For n = 1 to N (the maximum number of simulation runs)
6   /* Evaluation function value initialization */
     The U values of all cells are set to be 0.
7   Loop: For t = 1 to T (maximum index of time-slot)
8     Update U-value of current location: U = U +1
9     /* Select the available cell set for the new move */
      ACS (i.e., available cell set) = {cell(i, j): neighbors of current cell (include current cell itself) satisfying Acell(i, j, t+1) = 0}
10     Select untested cells UnTC from ACS: UnTC = {cell(i, j) with U(i, j) = 0;  cell(i, j) ∈ ACS}
11    If UnTC ≠ null
12       Select the cell with the smallest Prior value as the location of the next move
13    Else Select the cell with the smallest U value as the location of the next move
14    End if
15    Check if all cells have been tested. If yes, break;
16  End loop
17  Find the shortest path from the current location to the stopping point.
18  Record the test application time and the test plan
19 End loop
20 Find the test plan with the minimum test application time.
```

Fig. 14. Sketch of the MNCS algorithm.

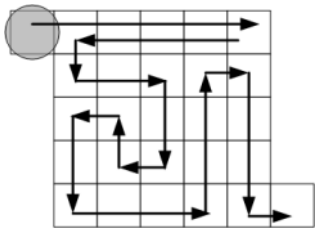

Fig. 15. The concurrent test plan obtained by the MNCS algorithm.

time-slot). Otherwise (i.e., it is a spare cell or a primary cell that will not be used in the assay in the future), we assign a large number to the *Prior* value for this cell. We greedily select the cell with the smallest *Prior* value from the untested neighboring cells. The introduction of the evaluation functions U and *Prior* adds more guidance to heuristically find efficient solutions for concurrent testing. The procedure of the MNCS algorithm is outlined in Figure 14. Due to the probabilistic nature of this approach, an adequate number of simulation runs (e.g., $\geq$ 1000) are needed to find an efficient solution, which leads to a relatively large computational time.

As an illustration, we apply the MNCS algorithm to the example of Figure 12. A concurrent test plan of 29 time-slots obtained through 1000 simulation runs is shown in Figure 15. It took 10 minutes of CPU time. The probabilistic searching in the MNCS algorithm can help to avoid the extreme case with the expense of the higher computation cost compared to the SP algorithm.

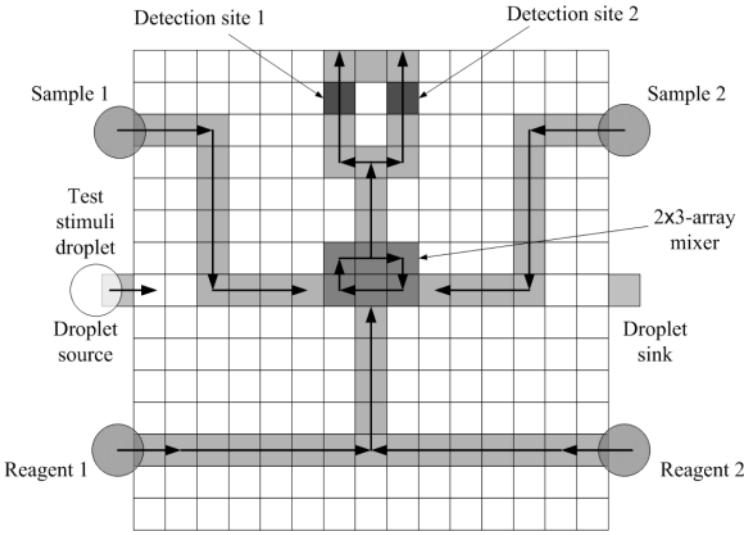

Fig. 16. Microfluidic array used for multiplexed biochemical assays.

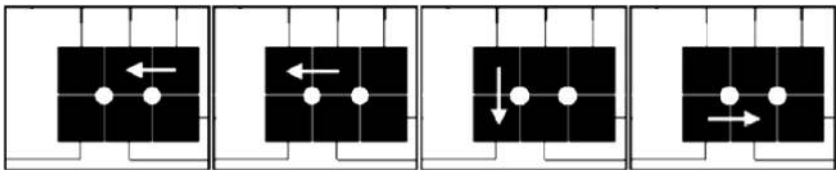

Fig. 17. Mixed droplet motion in a 2 × 3-array mixer.

7. EXAMPLE: CONCURRENT TESTING FOR MULTIPLEXED BIOASSAYS

In this section, we use a real-life example of multiplexed bioassays to illustrate how the proposed methods can be used for the concurrent testing. The multiplexed biochemical assays in the experiment consist of a glucose assay and a lactate assay based on colorimetric enzymatic reactions, which have been described in Section 2.

The digital microfluidic array used for this multiplexed bioassay is shown in Figure 16. The fabricated prototype was shown in Figure 3. In this system, the sample droplets containing Sample 1 (glucose) and Sample 2 (lactate), and the reagent droplets consisting of Reagent 1 (glucose oxidase, peroxidase, 4-AAP and TOPS) and Reagent 2 (lactate oxidase and other chemicals) are dispensed into a 15 × 15 microfluidic array (22.5mm × 22.5mm) from on-chip reservoirs, respectively. They are guided through the transportation paths, denoted by gray cells, when a 50 V actuation voltage with the frequency of 16 Hz is applied to the control electrodes. Droplets of the sample and the reagent are transported toward a mixer with a linear array design to mix together. In this 2 × 3-array mixer, the mixed droplet turns around two pivot points with a translational step in between; see Figure 17. In experiments, an average mixing time of 6 seconds was achieved at 16 Hz by rotating the droplet counter-clockwise in the 2 × 3 array [Paik et al. 2003].

Table III. Schedule of the Set of Multiplexed Bioassays

Time (second)	Operation
0	Sample 2 and Reagent 2 start to move towards the mixer.
0.8	Sample 2 and Reagent 2 begin to mix together and turn around in the 2×3-array mixer.
6.0	Sample1 and Reagent 1 start to move towards the mixer. Sample 2 and Reagent 2 continue the mixing.
6.8	Sample 2 and Reagent 2 finish the mixing and Product 2 leaves the mixer to optical detection location 2. Sample 1 and Reagent 1 begin to mix in the 2×3-array mixer.
12.8	Sample 1 and Reagent 1 finish the mixing and product 1 leaves the mixer to the optical detection location 1. Product 2 continues the absorbance detection.
19.8	Product 2 finishes optical detection and leaves the array to the waste reservoir. Product 1 continues the absorbance detection.
25.8	Product 1 finishes optical detection and leaves the array to the waste reservoir. One procedure of the multiplexed bioassays ends.

The enzymatic reactions are carried out during the mixing step. After this step, a droplet containing the product of the reaction (that is, Product 1), such as colored quinoneimine, is moved to the optical detection site, where the absorbance is measured for about 13 seconds using the LED-photodiode setup described in Section 2. Finally, the droplet leaves the microfluidic array to the waste reservoir. In this experiment, filler fluid of immiscible 1 cSt silicone oil is used to surround the droplet to prevent evaporation and reduce the droplet actuation voltage. A similar procedure is also used in the lactase assay (denoted as: Sample 2 + Reagent 2 $\rightarrow$ Product 2). These assays can be integrated on a microfluidic array to form a set of multiplexed biomedical assays for clinical diagnosis on metabolites. The schedule of this set of multiplexed assays is shown in Table III. In order to detect catastrophic faults in this system, such as electrode degradation, during field operation, we add a built-in test hardware to this system. The test hardware consists of droplet sources that generate and dispense the test droplet (e.g., 0.1 M KCL solution), and droplet sinks connected to an on-chip capacitive detection circuit. The goal of the concurrent testing is to ensure that the test droplet traverses every cell in this 15×15 array, that is, not only the spare cells, but also the cells used in the biomedical assay.

7.1 Modified ILP Method

Due to the inherent complexity of this optimization problem, the computational effort required by the ILP model increases dramatically for a microfluidic array of large size. Thus, it is hard to obtain an optimal solution for a 15×15 microfluidic array. However, we can modify the ILP method proposed in Section 5 to derive a close-to-optimal test plan for this example of a 15×15 array. We first partition the large array into nonoverlapping parts. Thus, a new array of the smaller size is formed, where each new cell represents a partition. For example, we can partition the 15×15 array in the example into nine nonoverlapping parts, and the overall system can now be viewed as a new 3×3 array; see Figure 18. Each partition, that is, the cell of the new small size array, consists

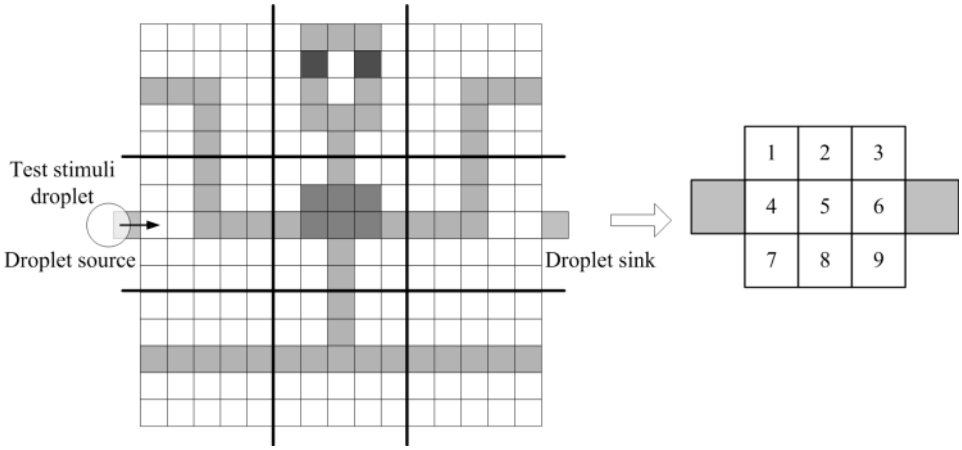

Fig. 18. Partition of a 15 × 15 array.

of 5 × 5 microfluidic cells. We then define the following operations that can be performed in the partition:

(1) *Transportation.* Sample droplets and reagent droplets move through one partition along five grid points (e.g., in cells 1, 3, 4, 6, 7, 8, 9). This operation takes 0.3 second, when a control voltage with the frequency of 16 Hz is applied.

(2) *Mixing.* Sample droplets mix with reagent droplets, and they move round a 2 × 3 array to accelerate the mixing procedure (e.g., in cell 5). The operation time is 6 seconds.

(3) *Optical Detection.* The absorbance of the droplet containing the colorimetric product of enzymatic reaction is detected by the LED-photodiode (e.g., in cell 2). The detection for an assay product takes 13 seconds.

(4) *Testing.* The test droplet sweeps all the microfluidic cells in this partition. The optimal testing time, obtained using the ILP model for a 5 × 5 array (a single partition) is 1.7 second; during this time, the test droplet traverses all 25 cells when a control voltage with the frequency of 16 Hz is applied.

We next apply the ILP scheduling model described in Section 5 to the 3 × 3 array obtained from the partitioning. We first modify the time-slot. The length of a modified time slot equals to the operation time of testing for one cell in the 3 × 3 array, that is, 1.7 second. In this way, we digitize the operation schedule of the multiplexed bioassay. When a partition cell is used in the operation of transportation, mixing, or optical detection during some time-slot, this cell is considered to be unavailable in this modified time-slot; see Table IV. Note that, except for the testing operation, each partition cell has a segregation region, which wraps round the functional operation region. This isolates the droplet operated in one partition from the droplets in the adjacent partitions. This implies that the test droplet can be traversing one partition, while the bioassay operation is being carried out in the adjacent partition. We then set $\sum_{(i,j)\in U_k} X_{ijkl} = 0$ for every modified time slot k, where U_k is the set of cells assigned to the assay operation in modified time slot k; this information is listed in Table IV.

Table IV. Cells Assigned to Assay Operation in Each Time Slot for the Multiplexed Assay

Modified Time-Slot	Time (seconds)	Cells Assigned to Assay Operation
1	(0–1.7)	3, 5, 6, 8, 9
2, 3	(1.7–5.1)	5
4	(5.1–6.8)	1, 4, 5, 7, 8
5, 6, 7, 8	(6.8–13.6)	2, 5
9, 10, 11, 12, 13, 14, 15, 16	(13.6–27.2)	2

Table V. Schedule for Concurrent Testing

Time-Slot	Fault Testing	Multiplexed Biochemical Assay	
1	Test droplet dispensed from the droplet source; testing partition cell 4 (sweeping all the microfluidic cells in the partition).	Sample 2 and reagent 2 transport through cells 3, 6 and cells 9, 8; then mix together in cell 5.	
2	Testing partition cell 1.	Sample 2 and reagent 2 continue the mixing in cell 5	
3	Testing partition cell 2.		
4	Testing partition cell 3.	Sample1 and reagent 1 move towards cell 5 through cells 1, 4 and cells 7, 8.	
5	Testing partition cell 6.	Sample 2 and reagent 2 finish the mixing and product 2 leave cell 5 to optical detection location 2 of cell 2. Sample 1 and reagent 1 begin to mix in cell 5.	
6	Testing partition cell 9.		
7	Testing partition cell 8.		
8	Testing partition cell 7.	Sample 1 and reagent 1 finish the mixing and product1 leave cell 5 to the optical detection location 1 of cell 2.	
9	Testing partition cell 4.	Product 2 performs optical detection; then leaves the array to the waste reservoir	Product 1 performs optical detection; then leaves the array to the waste reservoir.
10	Testing partition cell 5.		
11	Testing partition cell 6; Test droplet reaches the droplet sink →**Testing ends**		
12			
13			
14			
15			→
16			**Biomedical assay ends**

After the modification, the optimized result obtained using *lpsolve* for the 3×3 partition array is listed in Table V; this modified-ILP approach took 4 minutes of CPU time. It is shown that this test plan ensures that the fault testing is performed simultaneously with a multiplexed bioassay. The complete test procedure requires 11 modified time slots, that is, 18.7 seconds, and this is overlapped with one procedure of the multiplexed biomedical assay that takes 25.8 seconds. No delay is incurred due to the testing procedure. Note that if offline testing is carried out in a stand-alone manner, it needs 15 seconds. Although the testing time is less than that for concurrent testing, off-line testing requires the bioassay operation to be halted for 15 seconds. In contrast, the proposed concurrent testing method allows the normal biochip operation to be carried out continuously without the need for periodic interruption of the bioassay.

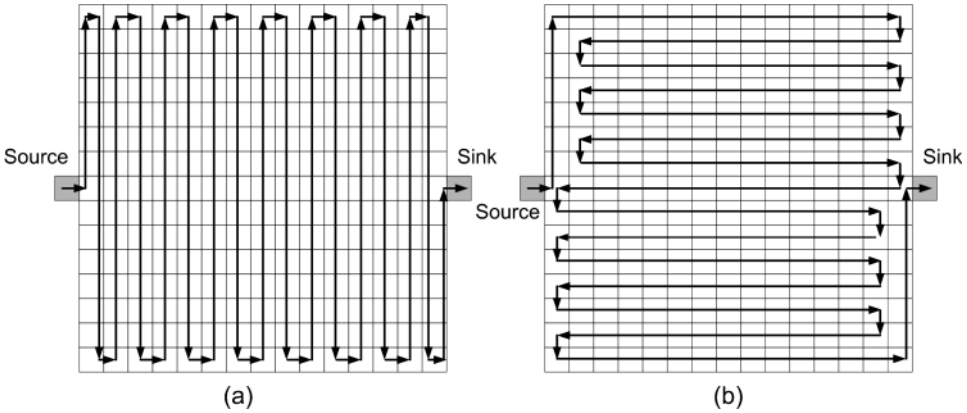

Fig. 19. Scanning paths used in the SP algorithm for the example.

Table VI. Ratios of the Heuristic Solutions to the Lower Bound

	Modified ILP	SP Algorithm (1)	SP Algorithm (2)	MNCS Algorithm
Heuristic result/LB	1.3	2.3	1.5	1.5

7.2 Results for Heuristic Methods

We next apply the two proposed heuristic methods to the example of 15 × 15 array to obtain the close-to-optimal testing schedules. Two different scanning paths are used in the SP algorithm, shown in Figure 19. Their corresponding concurrent testing times are 33.1 seconds and 21.4 seconds, respectively. The corresponding CPU times are 5 minutes and 3 minutes, respectively. Note that the testing time for the scanning path in Figure 19(a) is much higher than the path in Figure 19(b); in the first test plan, the test droplet has to wait until cells used for optical detection become available for testing. If the test droplet is guided along the path shown in Figure 19(b), it can visit the cells used for optical detection before they are occupied by the product droplets in the normal bioassay operation, thereby reducing the waiting time for the test droplet.

Finally, we use the MNCS algorithm to derive a feasible schedule; 5000 simulation runs are used in the experiment. The testing time is 21.5 seconds. The CPU time for the example is 25 minutes. To evaluate the heuristic solutions, we can set a lower bound (LB) on the optimal solution for concurrent testing to be 14.1 seconds, that is, the time taken by a test droplet to move across all 225 cells, since the test droplet should visit each cell in the 15 × 15 array at least once. The ratio of the heuristic solutions (including the result obtained by the modified ILP method) to the lower bound is listed in Table VI.

8. CONCLUSION

We have presented a novel concurrent testing methodology for detecting catastrophic faults in digital microfluidics-based biochips. An integer linear programming model for test planning and test resource optimization has been described. This model leads to minimum testing time for a given hardware

overhead needed for droplet-dispensing sources and capacitive sensing circuitry. Due to the $\mathcal{NP}$-complete nature of the problem, we have also developed two heuristic algorithms. We have applied the proposed concurrent test methodology to a droplet-based microfluidic array that was fabricated and used to perform glucose and lactate assays. We have shown that the test approach interleaves test application with the biomedical assays and it prevents resource conflicts on the array. The proposed approach is therefore directed to ensuring high reliability and high availability of bio-MEMS and lab-on-a-chip systems, as they are increasingly deployed for safety-critical applications.

ACKNOWLEDGMENTS

The authors thank Dr. Vamsee Pamula and Dr. Vijay Srinivasan of Advanced Liquid Logic, Inc., for sharing their insights on glucose and lactate assays.

REFERENCES

BALCH, T. AND ARKIN, R. 1993. Avoiding the past: a simple, but effective strategy for reactive navigation. In *Proceedings of the International Conference on Robotics and Automation*, 678–685.

BERKELAAR, M. lpsolve. Eindhoven Univ. Technol., Eindhoven, The Netherlands [Online]. Available at ftp://ftp.ics.ele.tue.nl/pub/lp_solve.

CHO, S. K., FAN, S. K., MOON, H., AND KIM, C. J. 2002. Toward digital microfluidic circuits: Creating, transporting, cutting and merging liquid droplets by electrowetting-based actuation. In *Proceedings of the IEEE Conference on MEMS*. IEEE Computer Society Press, Los Alamitos, CA, 32–52.

DAVIES, B. 1995. Robotics in minimally invasive surgery. In *Proceedings of the IEE Colloquium Through the Keyhole: Microengoneering in Minimally Invasive Surgery*, 5/1–5/2.

DEB, N. AND BLANTON, R. D. 2000. Analysis of failure sources in surface-micromachined MEMS. In *Proceedings of the IEEE International Test Conference*. IEEE Computer Society Press, Los Alamitos, CA, 739–749.

DEB, N. AND BLANTON, R. D. 2004. Multi-modal built-in self-test for symmetric microsystems. In *Proceedings of the IEEE VLSI Test Symposium*. IEEE Computer Society Press, Los Alamitos, CA, 139–147.

DHAYNI, AL, MIR, S. AND RUFER, L. 2004. MEMS built-in-self-test using MLS. In *Proceedings of the European Test Symposium*, 66–71.

DUMAS, N., AZAIS, F., LATORRE, L., AND NOUET, P. 2004. Electrically-induced thermal stimuli for MEMS testing. In *Proceedings of the European Test Symposium*, 60–65.

GRAHAM, R., LAWLER, E., LENSTRA, J., AND KAN, A. R. 1979. Optimization and approximation in deterministic sequencing and scheduling: A survey. *Ann. Disc. Math.* 5, 287–326.

HENNING, A. K. 1998. Microfluidic MEMS. In *Proceedings of the IEEE Aerospace Conference*. IEEE Computer Society Press, Los Alamitos, CA, 471–486.

HULL, H. F., DANILA, R., AND EHRESMANN, K. 2003. Smallpox and bioterrorism: Public-health responses. *J. Lab. Clin. Med. 142*, 221–228.

INTERNATIONAL TECHNOLOGY ROADMAP FOR SEMICONDUCTORS (ITRS), http://public.itrs.net/Files/2003ITRS/Home2003.htm.

KERKHOFF, H. G. 1999. Testing philosophy behind the micro analysis system. In *Proceedings of the SPIE: Design, Test and Microfabrication of MEMS and MOEMS*. 78–83.

KERKHOFF, H. G. AND ACAR, M. 2003. Testable design and testing of micro-electro-fluidic arrays. In *Proceedings of the IEEE VLSI Test Symposium*. IEEE Computer Society Press, Los Alamitos, CA, 403–409.

KERKHOFF, H. G. AND HENDRIKS, H. P. A. 2001. Fault modeling and fault simulation in mixed micro-fluidic microelectronic systems. *J. Elect. Test. Theory. Appl. 17*, 427–437.

KOLPEKWAR, A. AND BLANTON, R. D. 1997. Development of a MEMS testing methodology. In *Proceedings of the IEEE Inernational Test Conference*. IEEE Computer Society Press, Los Alamitos, CA, 923–931.

MIR, S., CHARLOT, B., AND COURTOIS, B. 2000. Extending fault-based testing to microelectromechanical systems. *J. Elect. Test. Theory Appl. 16*, 279–288.

PAIK, P., PAMULA, V. K., AND FAIR, R. B. 2003. Rapid droplet mixers for digital microfluidic systems. *Lab on a Chip 3*, 253–259.

POUL, J. 2002. Bioterrorism and biodefence, *J. Infect. 44*, 59–66.

POLLACK, M. G., FAIR, R. B., AND SHENDEROV, A. D. 2000. Electrowetting-based actuation of liquid droplets for microfluidic applications. *Appl. Phys. Lett. 77*, 1725–1726.

POLLACK, M. G., SHENDERO, A. D., AND FAIR, R. B. 2002. Electrowetting-based actuation of droplets for integrated microfluidics. *Lab on a Chip 2*, 96–101.

POLLACK, M. G., PAIK, P. Y., SHENDERO, A. D., PAMULA, V. K., DIETRICH, F. S., AND FAIR, R. B. 2003. Investigation of electrowetting-based microfluidics for real-time PCR applications. In *Proceedings of μTAS*. 619–622.

REN, H. AND FAIR, R. B. 2002. Micro/nano liter droplet formation and dispensing by capacitance metering and electrowetting actuation. *Technical Digest IEEE-NANO*, 36–38.

SCHULTE, T. H., BARDELL, R. L., AND WEIGL, B. H. 2002. Microfluidic technologies in clinical diagnostics. *Clinica Chimica Acta 321*, 1–10.

SRINIVASAN, V., PAMULA, V. K., POLLACK, M. G., AND FAIR, R. B. 2003a. A digital microfluidic biosensor for multianalyte detection. In *Proceedings of the IEEE Conference on MEMS*. IEEE Computer Society Press, Los Alamitos, CA, 327–330.

SRINIVASAN, V., PAMULA, V. K., POLLACK, M. G., AND FAIR, R. B. 2003b. Clinical diagnostics on human whole blood, plasma, serum, urine, saliva, sweat, and tears on a digital microfluidic platform. In *Proceedings of μTAS*, 1287–1290.

SRINIVASAN, V., PAMULA, V. K., AND FAIR, R. B. 2004. An integrated digital microfluidic lab-on-a-chip for clinical diagnostics on human physiological fluids. *Lab on a Chip 4*, 310–315.

SU, F. AND CHAKRABARTY, K. 2004. Architectural-level synthesis of digital microfluidics-based biochips. In *Proceedings of the IEEE International Conference on CAD*. IEEE Computer Society Press, Los Alamitos,CA, 223–228.

SU, F. AND CHAKRABARTY, K. 2005. Design of fault-tolerant and dynamically-reconfigurable microfluidic biochips. In *Proceedings of the Design, Automation and Test in Europe (DATE) Conference*. 1202-1207.

SU, F., OZEV, S., AND CHAKRABARTY, K. 2004. Test planning And test resource optimization for droplet-based microfluidic systems. In *Proceedings of the European Test Symposium*, 72–77.

SU, F., OZEV, S., AND CHAKRABARTY, K. 2005. Ensuring the operational health of droplet-based microelectrofluidic biosensor systems. *IEEE Sens. J. 5*, 763–773.

THORSEN, T., MAERKL, S., AND QUAKE, S. 2002. Microfluidic large-scale integration. *Science 298*, 580–584.

TRINDER, P. 1969. Determination of glucose in blood using glucose oxidase with an alternative oxygen acceptor. *Ann. Clin. Biochem. 6*, 24–27.

VENKATESH, S. AND MEMISH, Z. A. 2003. Bioterrorism: A new challenge for public health. *Int. J. Antimicro. Agents 21*, 200–206.

VERPOORTE, E. AND DE ROOIJ, N. F. 2003. Microfluidics meets MEMS, *Proc. IEEE 91*, 930–953.

Videos on droplet transport, dispensing, mixing and biomedical assays [Online]. Available at http://www.ee.duke.edu/Research/microfluidics

ZHANG, T., CHAKRABARTY, K., AND FAIRS, R. B. 2002. *Microelectrofluidic Systems: Modeling and Simulation.* CRC Press, Boca Raton, FL.

Received March 2005; revised July 2005 and August 2005; accepted August 2005